PERGAMON

International Journal of Solids and Structures 40 (2003) 5819–5837

INTERNATIONAL JOURNAL OF SOLIDS and STRUCTURES

www.elsevier.com/locate/ijsolstr

A cohesive plastic and damage zone model for dynamic crack growth in rate-dependent materials

Xi Zhang [a,*], Yiu-Wing Mai [b], Rob G. Jeffrey [a]

[a] *CSIRO Petroleum, P.O. Box 3000, Glen Waverley, VIC. 3150, Australia*

[b] *Centre for Advanced Materials Technology (CAMT), School of Aerospace, Mechanical and Mechatronic Engineering J07, The University of Sydney, Sydney, NSW 2006, Australia*

Received 22 November 2002

Abstract

Mode I steady-state dynamic crack growth in rate-dependent viscoplastic solids containing damage, under small scale yielding conditions, is analyzed based on a modified cohesive zone model. A multi-scale approach is used to describe the entire non-linear zone consisting of a plastic region and a damage region, each of which has its own constitutive law. Traction in the damage region is characterized by a softening power-law, in terms of the ultimate strength, a softening index and a rate sensitivity factor. In the plastic region, the cohesive law is assumed to be both strain hardening and rate dependent. The critical crack opening displacement at the physical crack-tip controls crack growth. The governing integral equations are derived and solved by a collocation method combined with associated boundary conditions. Numerical results are presented for the traction and opening profiles along the cohesive zone, the fracture energy and lengths of the damage and non-linear zones at different crack speeds and for different material parameters. The importance of factors, such as material softening, plastic deformation, crack speed and viscosity, is identified by parametric studies. In addition, the competition of plastic flow and material damage, and its effect on crack growth, are discussed.

Keywords: Dynamic crack growth; two-zone cohesive model; Damage softening; Rate dependence; Crack-tip constraint

1. Introduction

Many engineering materials display so-called 'strain softening' behavior as microstructures evolve. For instance, ductile crack growth in metals is usually accompanied by a decrease in strength caused by the nucleation and growth of voids. Cracked specimens have, at least locally, a non-linear characteristic zone in the crack-tip vicinity. Material elements in this zone cannot sustain further load. This phenomenon is also common in other materials such as polymers, coarse-grained ceramics, and fiber composite

* Corresponding author. Tel.: +61-3-9259-6888; fax: +61-3-9259-6900.
E-mail address: xi.zhang@csiro.au (X. Zhang).

0020-7683/$ - see front matter © 2003 Elsevier Ltd. All rights reserved.
doi:10.1016/S0020-7683(03)00370-6

materials. Strictly speaking, conventional macroscopic continuum descriptions of this highly deformed zone are not appropriate. Barenblatt (1959), Dugdale (1960) and Bilby et al. (1963) introduced a cohesive zone concept by assuming a relationship between the cohesive force and the pseudo opening displacement. However, the lack of strain-softening response in the B–D (Bareblatt–Dugdale) model results in stress divergence and discontinuity at the receding edge of the cohesive zone, as shown by Glennie (1971). Hence, correct modeling of the fracture behavior of these materials depends very much on the intimate knowledge of their failure micro-mechanisms and certain internal structures. Stable crack growth in strain-softening materials has been studied for fiber reinforced materials by Foote et al. (1986) and Cui (1995), for laminated composites by Wnuk and Kriz (1985), for rate-dependent materials by Fager et al. (1991) and for ductile materials by Tvergaard and Hutchinson (1992), Zhang and Gross (1995) and Yuan et al. (1996).

The cohesive zone, with its own constitutive requirement, is confined to a line segment or a narrow strip ahead of the crack-tip. Use of a cohesive zone has successfully captured some main features of fracture behavior such as vanishing stress singularity, finite fracture process zone and increasing toughness at high crack growth rates. Although recent work by Costanzo and Walton (2002) did consider the dynamic crack growth in materials with coupled thermal and mechanical responses, few studies addressed the co-existence of different mechanisms inside the cohesive zone, such as strain-hardening plastic flow and strain-softening void growth and coalescence. Clearly, material points ahead of the crack-tip are either cohesive or decohesive. Once in a decohesive state, they cannot return to their original cohesive state. In fact, most studies based on the original B–D model do not separate the damage zone or the fracture process zone from the entire non-linear region, even though a combined plastic/damage cohesive law was presented by Zhang and Gross (1995). Thus, it is difficult to discern macroscopic behaviors caused by damage from those by plastic deformation. Many experimental results (e.g., Yuan et al. (1996) and cited references therein) have shown that the damage zone in a ductile material is restricted to a very small region near the physical crack-tip. However, this small damage zone can cause a considerable increase in the fracture resistance. In some extreme cases, there is no damage zone, only plastic flow. Hence, it is necessary to examine the cohesive zone from a multi-scale point of view, especially for a small damage zone lying between the crack-tip and the plastic zone. Wnuk (1983) modified the B–D model by using two zones so as to predict the stability of crack growth based on their relative lengths, although the transition from plastic to damage zone is expected to be gradual. The two extremes, very brittle and very ductile, can be described as two limiting cases corresponding to a fully damage zone and a pure plastic zone ahead of the crack-tip, respectively. Consideration of crack growth stability based on length scales has been highlighted in recent works for new materials with coupled mechanisms (Cox and Marshall, 1994; Gao et al., 1997). Of course, the need to adopt a two-zone cohesive model also lies in the difficulty in developing a unified model covering all stages of material deformation.

Fracture characteristics for ductile materials can be represented by a combined cohesion–decohesion curve. Fig. 1 shows the typical curve for a unit cell subjected to uniaxial straining. It is always considered as a model in the cohesive zone of a Mode I crack. Material elements experience decohesion when the crack opening $\delta > \delta_1$ (the opening corresponding to the peak cohesive stress) while cohesion by plastic deformation takes place when $\delta < \delta_1$. In addition, when the cohesive stress $p < \sigma_E$ (yield strength) and for small opening displacement, there is a non-dissipative regime. However, the energy dissipated in the non-dissipative zone is not considered in this paper. While ductile fracture is different from failure of piezoelectric ceramics with coupled electrical–mechanical behaviors (Gao et al., 1997), damage and plastic deformation can also be taken as two different deformation mechanisms, as stated above. Plastic flow by itself has some special characteristics such as strain hardening and elastic unloading, and post-peak localization caused by void growth can limit plastic deformation. Crack growth in ductile materials is governed by the competition between damage and plastic flow. Both contribute to the fracture energy, but compete against each other. Two critical parameters in the cohesive laws control the fracture process. One

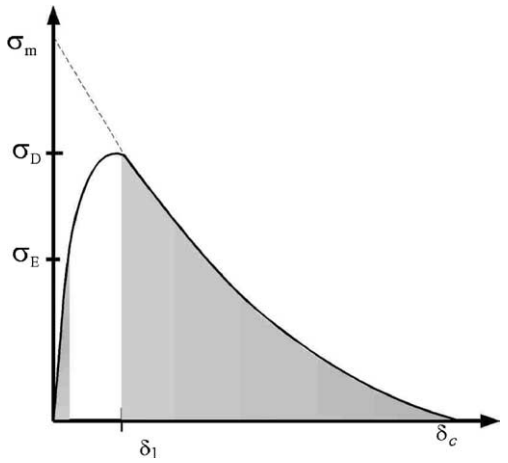

Fig. 1. Typical curves for the cohesion–decohesion behaviors of ductile materials based on the unit-cell model subject to uniaxial stress.

is the cohesive strength σ_D in Fig. 1, which is the peak stress at instability under load-controlled condition. The higher the cohesive strength, the smaller is the fracture process zone as found by Tvergaard and Hutchinson (1992). Another parameter is the shape of the cohesion–decohesion curve. The curve shape influences the ratio of the height of the process zone to its length, as observed by Andersson and Bergkvist (1970).

The cohesion–decohesion curve is also affected by some macroscopic parameters such as crack-tip constraints resulting from specimen geometry and loading mode. The constraint effect has been dealt with in two ways: macro-mechanical and micro-mechanical. Macro-mechanical approaches by Hancock et al. (1993) and O'Dowd and Shih (1991) used additional parameters, like T-stress or Q-term, to identify the constraint effect. Alternatively, the curves from the unit-cell model under multi-axial tension can approximately reflect the real situation of void growth ahead of the crack-tip. Micro-mechanical approaches have established a range of damage models, such as the modified Gurson model (see Tvergaard, 1990), to account for the effect of hydrostatic stresses. A negative T-stress can extend the value of δ_1, and hence, low constraints can make the process zone deeply embedded inside the plastic region, as argued by Broberg (1999). Recent work by Wnuk and Legat (2002) has included a triaxility-dependent cohesive zone model to assess fracture work and cohesive stress distributions because low constraint can reduce the value of σ_D.

It is anticipated that introduction of a two-region cohesive zone model would be reasonable to generalize the essential ideas of Barenblatt (1959) and Dugdale (1960), though the corresponding non-linear analysis becomes more difficult. As a first step to understand failure mechanisms, some simple forms of cohesive constitutive laws are used. While the two-zone model is more difficult to judge than the original B–D model, the results will shed new lights on our understanding of the crack problem.

The issue of Mode I steady-state dynamic crack growth in rate-dependent viscoplastic materials containing damage under small scale yielding, is revisited based on a two-region cohesive zone model. This paper is organized as follows. In Section 2, formulation of steady-state dynamic growth of a plane-strain mode I crack under small scale yielding conditions is given and the cohesive laws in the damage zone and the plastic zone are provided. This is followed in Section 3 by derivations of the governing equations based on the balance of tractions along the cohesive zone. The numerical method used to solve the integral equation is given in Section 4 and numerical results for a system of material parameters and crack growth rates are presented in Section 5 for different crack speeds. Concluding remarks are given in Section 6.

2. Statement of the problem

Consider the problem of a steady-state plane strain mode I semi-infinite crack spreading dynamically in an isotropic elastic medium under small scale yielding conditions. The crack lies on the plane $y = 0$ and extends in the x-direction at a constant crack speed V with the origin of the coordinates moving with the crack-tip. The singular opening stresses ahead of the crack-tip can be characterized by a Mode I dynamic stress intensity factor K_∞ in the form

$$\sigma(x) = \frac{K_\infty}{\sqrt{2\pi x}} \tag{1}$$

so that K_∞ represents the level of external loads.

To account for non-linearity in viscoplastic materials, we resort to the cohesive zone model as emphasized in the previous section. Ahead of the crack-tip, there is a cohesive zone, that is, a non-linear region across which the cohesive forces can be translated. The geometric configuration of the model is schematically illustrated in Fig. 2. The entire cohesive zone is divided into two regions to avoid inconsistency with experimental observations. There are different micro-mechanisms operative in these two regions. One is void-damage softening and the other is plastic deformation hardening associated with mobile dislocations. Elastic behavior is maintained outside of the non-linear region. The cohesive-zone length is L. Region $0 < x < D$ represents the damage zone, the length of which is D. Region $D < x < L$ denotes the active plastic zone in which a hardening traction law is assigned.

The crack is treated with a cohesive stress $p(x)$ along the entire line segment of the effective crack. The opening displacement δ of the cohesive zone, corresponding to the responses of the cohesive stress, is defined as:

$$\delta(x) = u_y(x, +0) - u_y(x, -0) \tag{2}$$

in which u_y is the vertical displacement along the crack-face.

To obtain the mechanical response at given loads, a relation between the traction and the separation should be provided. In the remainder, a specified constitutive relation for power-law strain softening and rate sensitivity is chosen for the damage zone $[0, D]$. Its rate-independent form is illustrated in Fig. 3. We begin with a class of viscous cohesive laws in the form:

$$p(\delta) = \sigma_m \left(1 - \frac{\delta}{\delta_c}\right)^m (1 + \beta_m \dot{\delta}) \tag{3}$$

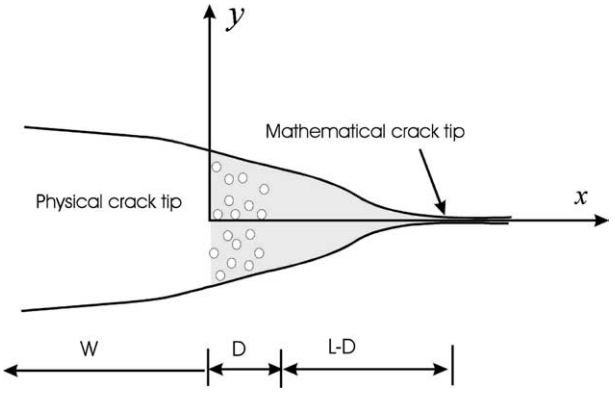

Fig. 2. Schematic of a cohesive zone ahead of a crack tip and the coordinate system.

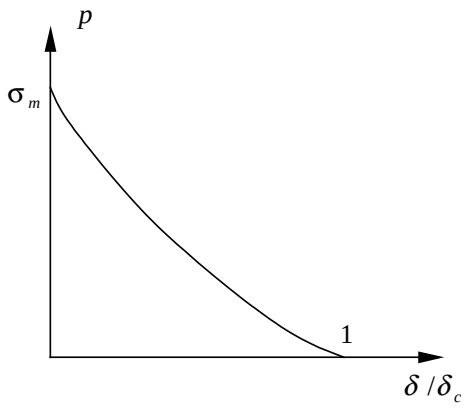

Fig. 3. Traction–separation law for a damaged material.

where m is softening index, β_m viscous coefficient due to inertia effect, δ_c critical opening displacement, σ_m ultimate tensile strength for the damage zone, and $\dot{\delta}$ rate of opening which relates to δ through the universal relationship for steady crack growth at a subsonic speed V:

$$\dot{\delta} = -V\frac{\partial \delta}{\partial x} \tag{4}$$

A hardening traction–separation relation is assigned to the plastic zone $[D, L]$. Its rate-independent form is shown in Fig. 4. The detailed expression is written as

$$p(\delta) = \sigma_{\mathrm{pl}}\left(\frac{\delta}{\delta_{\mathrm{c}}}\right)^{n}(1 + \beta_n\dot{\delta}) \tag{5}$$

where n is hardening exponent, σ_{pl} ultimate strength and β_n viscosity for plastic deformation. It is noted that the cohesive law in the plastic zone is also rate dependent, but with a different viscosity coefficient because of different mechanisms. This rising stress regime corresponds to dynamic dislocation movement. n can vary under the condition of $m > n$. It must be emphasized that β_m and β_n highlight the effect of material inertia. In their absence, the above laws are reduced to their rate-independent forms. For rate-dependent

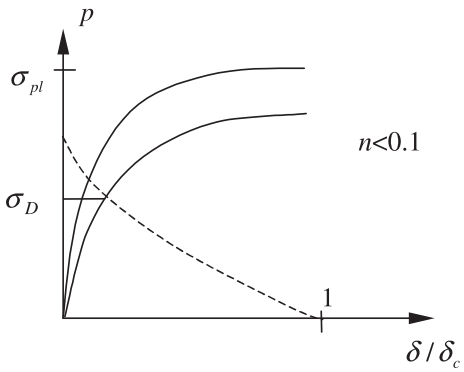

Fig. 4. Traction–separation law for plastic flow.

materials, the maximum cohesive stress σ_D depends not only on the cohesive material parameters in Eqs. (3) and (5), but also on the crack propagation rates from Eq. (4).

Then, we must decide on the boundary conditions and interface condition between the two zones. Material elements at the physical crack-tip lose their load-carrying ability. Therefore, the failure criterion is defined by:

$$\delta(x=0)=\delta_{\mathrm{c}} \tag{6}$$

It is assumed that the fracture process is dominated by non-linear deformation, that is, the area beneath the non-dissipative part in the cohesion–decohesion curve shown in Fig. 1 is extremely small. To meet this requirement, the crack opening at the leading edge should be extremely small. The traction at the leading edge is not necessarily zero and it may be comparable to its counter-parts in the plastic and damage zones. Therefore, it is assumed that

$$p(x=L)=\sigma_{\mathrm{G}} \quad \text{and} \quad \delta(x=L)\to 0 \tag{7}$$

where σ_{G} is minimum cohesive stress for occurrence of plastic deformation and it is dependent on the T-stress and loading modes. Considering Eqs. (5) and (7), a very small value of n ($=0.1$) should be used.

In addition, the stress and opening continuity should be maintained at the interface between two zones. Thus

$$p(x=D-0)=p(x=D+0) \tag{8}$$

$$\delta(x=D-0)=\delta(x=D+0) \tag{9}$$

The problem can also be studied from the energetic viewpoint. Energy release rate can be obtained by evaluating the dynamic J-integral along a remote contour Γ_{c} enclosing the whole cohesive zone $\Gamma_{\mathrm{d}}+\Gamma_{\mathrm{pl}}$, as shown in Fig. 5. Γ_{pl} and Γ_{d} denote the plastic and damage segments. It should be pointed out that the energy flux must also include the non-dissipative part, that is, the segment with $p<\sigma_{\mathrm{G}}$. In accordance with Griffith's theory, the non-dissipative cohesive stress yields the intrinsic fracture energy dissipated at a point-like sharp tip. However, the contribution from this non-dissipative stress is extremely small based on Eq. (7). The non-dissipative segment should be extremely small and it is not taken into account in this paper.

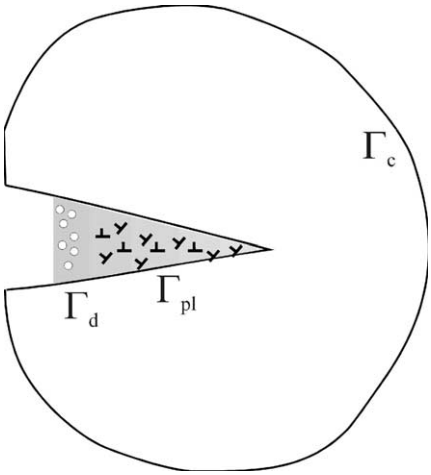

Fig. 5. J-integral contours for evaluating local and global energy fluxes.

Thus, the energy flux is approximately the rate of energy dissipated in the dissipative cohesive zone. From Freund (1990) the energy flux for steady-state dynamic crack growth is defined as

$$\dot{E} = V \int_{\Gamma_c} \left[(U+T)n_1 - \sigma_{ij} n_j \frac{\partial u_i}{\partial x} \right] \mathrm{d}s \tag{10}$$

in which U is strain energy density, T is kinetic energy density, n_i is normal unit of the contour and σ_{ij} and u_i are stress tensor and displacement vector, respectively.

To facilitate discussion, the ratio of energy flux to the crack speed is used, instead of the energy flux itself. Eq. (10) is rewritten as $\dot{E} = V E_\infty$, in which E_∞ is interpreted as the *available* energy release rate for the system. Since the linearly elastic material outside the cohesive zone is energy-conservation, the value of energy flux can be evaluated along the cohesive zone. Therefore, we have

$$\dot{E} = \int_0^L p(x)\dot{\delta}(x)\,\mathrm{d}x = -V \int_0^L p(x) \frac{\partial \delta(x)}{\partial x}\,\mathrm{d}x \tag{11}$$

We can also define the *required* energy release rate E_f for crack propagation, or called as the fracture energy dissipated in the cohesive zone. Since elastic energy is fully converted to fracture energy in the system, the *required* energy release rate must be identified with the *available* energy release rate. Thus, the fracture energy can be written as

$$E_f = -\int_{\Gamma_{pl}+\Gamma_d} p(x) \frac{\partial \delta(x)}{\partial x}\,\mathrm{d}x = -\left(\int_{\Gamma_{pl}} + \int_{\Gamma_d} \right) p(x) \frac{\partial \delta(x)}{\partial x}\,\mathrm{d}x \tag{12}$$

To compare the contributions from the damage and plastic zones, we denote E_d and E_{pl} the damage and plastic parts of the fracture energy, respectively.

3. Governing equations

According to dislocation theory, the dislocation density $\xi(x)$ is defined as the gradient of the jump of the crack profile, i.e., $\xi(x) = -\partial\delta(x)/\partial x$, and the crack opening displacement along the cohesive zone is given by

$$\delta(x) = \int_x^L \xi(t)\,\mathrm{d}t + \delta(L) \tag{13}$$

in which $\delta(L)$ is the opening at the leading edge of the non-linear zone. At the physical crack-tip, the critical crack opening displacement is

$$\delta_c = \int_0^L \xi(t)\,\mathrm{d}t + \delta(L) \tag{14}$$

Under plane strain conditions, the force at the location x caused by steady growth of an edge dislocation with unit Burger vector at location x_0 without tension (Weertman, 1996) is

$$\sigma_y(x) = -\frac{\mu f(V)}{x - x_0} \tag{15}$$

where V is the velocity of the gliding dislocations and $f(V)$ is a function of the velocity as

$$f(V) = -\frac{1}{2\pi\alpha_d} \frac{c_s^2}{V^2} [(1+\alpha_s^2)^2 - 4\alpha_d\alpha_s] \tag{16}$$

where $\alpha_d = (1 - V^2/c_d^2)^{1/2}\alpha_s = (1 - V^2/c_s^2)^{1/2}$, c_s and c_d are velocities of longitudinal and shear waves, respectively. In terms of Lame constants λ and μ, these characteristic speeds are $c_d = \sqrt{(\lambda + 2\mu)/\rho}$ and $c_s = \sqrt{\mu/\rho}$ in which ρ is the mass density.

The accumulated force from the distribution of dislocations along the entire inelastic zone for a semi-infinite crack is

$$\sigma_y = \mu f(V) \int_0^L \frac{\xi(t)}{x - t} \sqrt{\frac{t}{x}} \mathrm{d}t \tag{17}$$

The equilibrium of the motion of growing cracks is accounted for by the three force sources in the cohesive zone: (1) the opening stress without the cohesive zone (Eq. (1)), (2) the cohesive stress $p(x)$ and (3) the stress caused by dislocation $\sigma_y(x)$. This leads to:

$$p(x) = \frac{K_\infty}{\sqrt{2\pi x}} + \sigma_y(x) \tag{18}$$

Substituting Eqs. (17) into (18) results in the governing equation for the crack growth problem. Following Fager et al. (1991), Eq. (18) is rewritten as

$$p(x) = \frac{1}{\sqrt{2\pi x}} \left[K_\infty - \sqrt{2\pi}\mu f(V) \int_0^L \frac{\xi(t)}{\sqrt{t}} \mathrm{d}t \right] + \mu f(V) \int_0^L \frac{\xi(t)}{x - t} \sqrt{\frac{x}{t}} \mathrm{d}t \tag{19}$$

Since the stress at the physical crack-tip is finite, that is, $\lim_{x\to 0} \sqrt{x} p(x) = 0$, we obtain

$$K_\infty = \sqrt{2\pi}\mu f(V) \int_0^L \frac{\xi(t)}{\sqrt{t}} \mathrm{d}t \tag{20}$$

Thus, the cohesive stress *versus* dislocation density relation can be rewritten as

$$p(x) = \mu f(V) \int_0^L \frac{\xi(t)}{x - t} \sqrt{\frac{x}{t}} \mathrm{d}t \tag{21}$$

Based on the formulae in Muskhelishvili (1953), the above equation can be inverted. This leads to

$$\xi(x) = \frac{1}{\pi^2 \mu f(V)} \int_0^L \frac{\sqrt{L - t}}{\sqrt{L - x}} \frac{p(t)}{t - x} \mathrm{d}t + \frac{C}{\sqrt{L - x}} \tag{22}$$

in which C is a constant to be determined. Moreover, Eq. (22) can be recast as

$$\xi(x) = \frac{1}{\pi^2 \mu f(V)} \int_0^L \frac{\sqrt{L - x}}{\sqrt{L - t}} \frac{p(t)}{t - x} \mathrm{d}t + \frac{1}{\sqrt{L - x}} \left[C - \frac{1}{\pi^2 \mu f(V)} \int_0^L \frac{p(t)}{\sqrt{L - t}} \mathrm{d}t \right] \tag{23}$$

Also, Dugdale's condition, $\lim_{x\to L} \sqrt{L - x}\xi(x) = 0$, is applied at the leading edge of the cohesive zone. Hence, we have

$$C = \frac{1}{\pi^2 \mu f(V)} \int_0^L \frac{p(t)}{\sqrt{L - t}} \mathrm{d}t \tag{24}$$

The above equality is also called the Barenblatt's condition. It is used to determine the length of the cohesive zone.

Thus, the expression for dislocation density is reduced to

$$\xi(x) = \frac{1}{\pi^2 \mu f(V)} \int_0^L \frac{\sqrt{L - x}}{\sqrt{L - t}} \frac{p(t)}{t - x} \mathrm{d}t \tag{25}$$

By substituting Eqs. (25) in (20), the dynamic stress intensity factor becomes

$$K_\infty = \sqrt{\frac{2}{\pi}} \int_0^L \frac{p(t)}{\sqrt{L-t}}\,\mathrm{d}t \tag{26}$$

The fracture energy can be obtained by substituting Eqs. (25) in (12). Thus,

$$E_\mathrm{f} = \frac{1}{\pi^2 \mu f(V)} \left[\int_0^L \frac{p(t)}{\sqrt{L-t}}\,\mathrm{d}t \right]^2 \tag{27}$$

It is interesting to note that there exists a relationship between E_f, K_∞ and C. Using Eqs. (24), (26) and (27), it follows that

$$E_\mathrm{f} = \frac{K_\infty^2}{2\pi\mu f(V)} = \pi^2 \mu f(V) C^2 \tag{28}$$

Therefore, Eq. (24) can be replaced by Eq. (27) to calculate the size of the cohesive zone.

In addition, using Eq. (13) and integrating Eq. (25) with respect to x, it leads to the expression for the crack opening

$$\delta(x) = \frac{1}{\pi^2 \mu f(V)} \int_0^L p(t) \left[\frac{2\sqrt{L-x}}{\sqrt{L-t}} - \ln \left| \frac{\sqrt{L-x}+\sqrt{L-t}}{\sqrt{L-x}-\sqrt{L-t}} \right| \right] \mathrm{d}t + \delta(L) \tag{29}$$

From Eqs. (25) and (29), the crack opening displacement and its gradient are fully determined by the traction distribution along the cohesive zone.

It is convenient to rewrite all the equations in non-dimensional forms. Thus, by introducing the dimensionless coordinates:

$$\zeta = x/L \quad \text{and} \quad \eta = t/L \tag{30}$$

all the governing equations in terms of dislocation density can be expressed as follows.

Dislocation density governing equation:

$$\xi(\zeta) = \frac{\varepsilon_m}{\pi^2 f(V)} \int_0^1 \frac{\sqrt{1-\zeta}}{\sqrt{1-\eta}} \frac{\bar{p}(\eta)}{\eta-\zeta}\,\mathrm{d}\eta \tag{31}$$

Opening displacement governing equation:

$$\bar{\delta}(x) = \int_\zeta^1 \xi(t)\,\mathrm{d}t + \bar{\delta}(1) \tag{32}$$

Dugdale's condition:

$$\overline{E}_\mathrm{f} = \frac{\pi}{\pi^2 f(V) \bar{\delta}_\mathrm{c}} \left[\int_0^1 \frac{\bar{p}(\eta)}{\sqrt{1-\eta}}\,\mathrm{d}\eta \right]^2 \tag{33}$$

Cohesive zone constitutive equations:

$$\bar{p}(\eta) = \begin{cases} \left(1 - \dfrac{\bar{\delta}(\eta)}{\bar{\delta}_\mathrm{c}}\right)^m (1 + \beta_m V \xi(\eta)) & 0 < \eta < \overline{D} \\ \alpha \left(\dfrac{\bar{\delta}(\eta)}{\bar{\delta}_\mathrm{c}}\right)^n (1 + \beta_n V \xi(\eta)) & \overline{D} < \eta < 1 \end{cases} \tag{34}$$

Fracture criterion:

$$\bar{\delta}(0) = \bar{\delta}_c \tag{35}$$

Boundary conditions at the leading edge:

$$\bar{p}(1) = \frac{\sigma_G}{\sigma_m} \quad \text{and} \quad \bar{\delta}(1) = 0 \tag{36}$$

Continuity on the interface between two zones:

$$\bar{p}_1(\overline{D} - 0) = \bar{p}_2(\overline{D} + 0) \tag{37}$$

$$\bar{\delta}_1(\overline{D} - 0) = \bar{\delta}_2(\overline{D} + 0) \tag{38}$$

where $\bar{\delta} = \delta/L$ is normalized crack opening; $\bar{\delta}_c = \delta_c/L$ and as δ_c is specified, $\bar{\delta}_c$ represents the length of the cohesive zone; $\bar{p} = p/\sigma_m$ is normalized cohesive stress; $\bar{p}_i$ and $\bar{\delta}_i$ $(i = 1, 2)$ denote the normalized cohesive stress and opening on the interface calculated based on the cohesive laws in two zones, respectively; $\varepsilon_m = \sigma_m/\mu$ is a reference strain in the damage zone; $\overline{D} = D/L$ is the length ratio of the damage zone to the cohesive zone; $\alpha = \sigma_{pl}/\sigma_m$ is the stress ratio between two zones; the normalized fracture energy is defined as:

$$\overline{E}_f = \frac{E_f}{\sigma_m \varepsilon_m \delta_c} \tag{39}$$

Similarly, the normalized plastic and damage components of the fracture energy are expressed as:

$$\overline{E}_{pl} = \frac{E_{pl}}{\sigma_m \varepsilon_m \delta_c} \quad \text{and} \quad \overline{E}_d = \frac{E_d}{\sigma_m \varepsilon_m \delta_c} \tag{40}$$

4. Numerical scheme

A collocation method is applied to solve the above system of integral equations (31)–(38). It is assumed that intervals, $[0, \overline{D}]$ and $[\overline{D}, 1]$, are divided into M and N uniform-sized elements, respectively. The unknown crack opening $\bar{\delta}_i$ and its gradient ξ_i are assumed constant in each element; and so are the cohesive forces $\bar{p}_i$. Furthermore, the mid-point of each element is taken as the collocation points. Thus, a system of non-linear algebraic equations can be obtained:

$$\xi_i - \frac{\varepsilon_m}{\pi^2 f(V)} \sum_{j=1}^{M+N} B_{ij} \bar{p}_j(\eta_j) = 0 \tag{41}$$

$$\bar{\delta}_i = \sum_{j=i}^{M+N} \xi_j \Delta\eta_j \tag{42}$$

$$\overline{E}_f = \frac{1}{\pi^2 f(V) \bar{\delta}_c} \left[\sum_{i=1}^{M+N} C_i \bar{p}_i(\zeta_i) \right]^2 \tag{43}$$

in which

$$\bar{p}(\eta_j) = \begin{cases} \left(1 - \dfrac{\bar{\delta}_j}{\bar{\delta}_c}\right)^m (1 + \beta_m V \xi_j) & 0 < \eta_j < \overline{D} \\ \alpha \left(\dfrac{\bar{\delta}_j}{\bar{\delta}_c}\right)^n (1 + \beta_n V \xi_j) & \overline{D} < \eta_j < 1 \end{cases} \tag{44}$$

and

$$B_{ij} = \left[-\ln\left|\frac{\sqrt{1-\zeta_i}+\sqrt{1-\eta}}{\sqrt{1-\zeta_i}-\sqrt{1-\eta}}\right|\right]\Bigg|_{\eta_j}^{\eta_{j+1}} \tag{45}$$

$$C_i = -2\sqrt{1-\eta}\Big|_{\eta_i}^{\eta_{i+1}} \tag{46}$$

Considering Eqs. (41) and (43) plus the traction continuity at $\overline{D}$ and the failure criterion Eq. (35), we have $M+N+3$ equations for $M+N$ unknown opening gradients and $\bar{\delta}_c$, $\overline{D}$ and $\overline{E}_f$. With known values of the opening gradients, the normalized crack opening $\bar{\delta}_i$ can be obtained through Eq. (42). Thus, the opening continuity on the interface is automatically met. The opening at the leading edge vanishes based on Eq. $(30)_2$. In addition, the specified traction at the leading edge (i.e., Eq. $(30)_1$) of the cohesive zone is imposed by assigning it to the leading element. In the calculations, it is found that the crack opening and its gradient for the leading element are extremely small.

The non-linear algebraic equations are solved numerically using the Newton–Raphson method (Press et al., 1992). Accordingly, the iteration stops when the following norm is less than 10^{-24},

$$\|g\| = \sum_{i=1}^{M+N+3} (|g_i|)^2 \tag{47}$$

in which g_i is the residual values of the right-hand and left-hand sides in Eqs. (41) and (43), of the tractions at $\overline{D}$ approaching from two zones and of $\bar{\delta}(0)$ and $\bar{\delta}_c$.

It should be noted that the convergence of the Newton–Raphson method depends on the choice of trial solutions. Owing to the sudden change in the constitutive laws, difficulty arises in the numerical method regarding convergence. Here, we follow the same solution strategy used by Costanzo and Walton (2002). The solutions for some parameters are used as the initial guess for the next solution with small changes in parameters.

5. Numerical results

Numerical calculations were carried out for steady-state dynamic propagation of plane-strain mode I cracks. Element numbers, $M = 30$ and $N = 60$, were used, to satisfy the solution accuracy requirements. The elastic properties are $E = 200$ GPa, $\nu = 0.3$. The mass density is 7833 kg/m^3. The longitudinal and shear wave speeds of the material are 5862.7 and 3133.7 m/s, respectively. The corresponding Rayleigh wave speed is 2902.3 m/s. The choice of m and n ($=0.1$) is such that plastic deformation is a major source of energy dissipation in ductile materials (see, Yuan et al., 1996). For simplicity, it is assumed that the material possesses the same viscosities in the damage and plastic regimes, that is, $\beta = \beta_m = \beta_n$. The ultimate strength for the damage cohesive law is taken as 1200 MPa. The value of σ_G is specified as $0.5\sigma_m$ in the calculations.

5.1. Crack speeds

We begin with the influence of crack speeds on the variations of the cohesive behavior at the crack-tip. The material constants are $\alpha = 1$, $\beta = 0.002$ and $m = 0.3$. Fig. 6a–c show distributions of the normalized crack opening $\bar{\delta}$, its gradient ξ and the normalized traction $\bar{p}$ along the length of the cohesive zone. Continuity in these curves is clear although two different material properties are employed. It is noted that all curves are smooth and the given traction at the leading edge of the cohesive zone is satisfied accurately. Very low values of opening and opening rate at the leading edge indicate a vanishing source of the fracture energy outside the cohesive zone and a finite cohesive stress as shown in Fig. 6a and b. In combined plastic

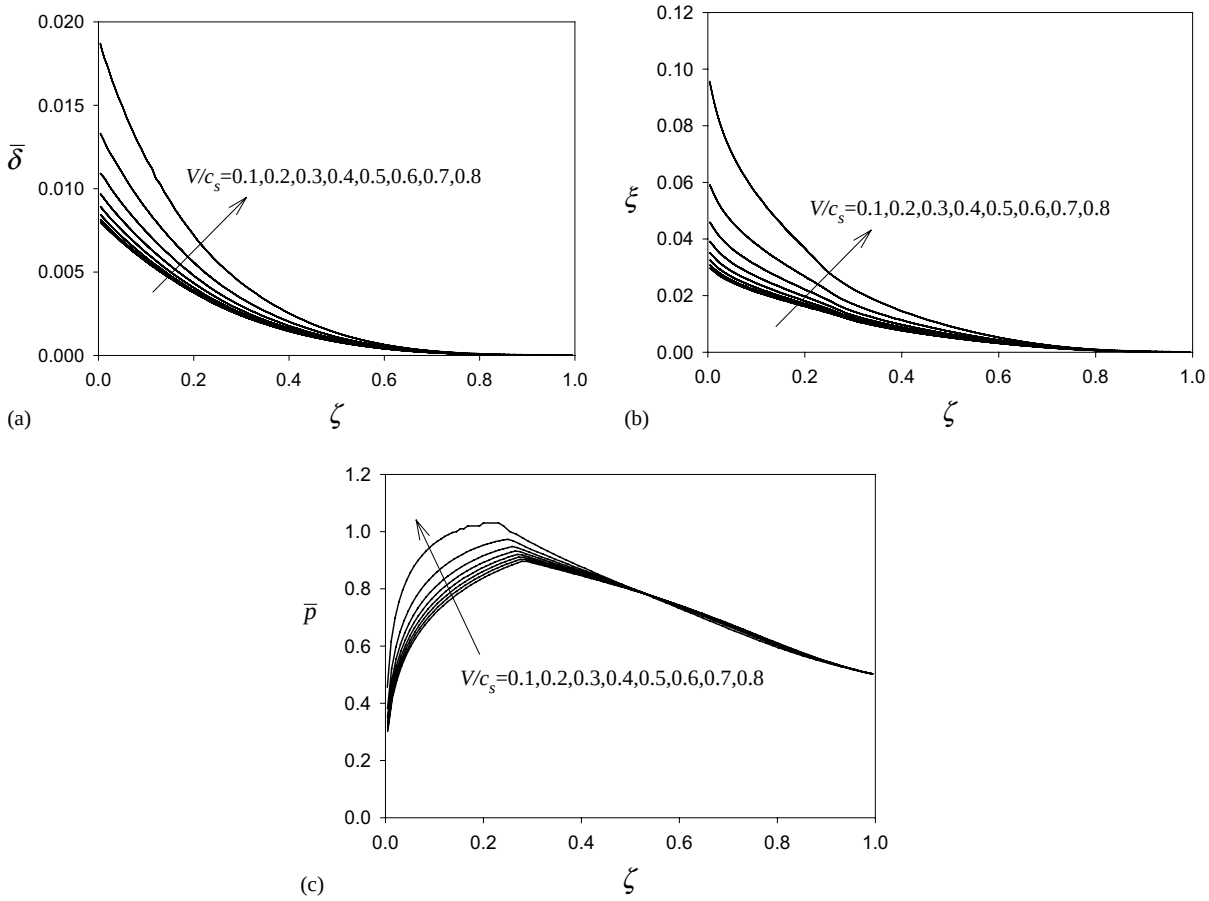

Fig. 6. Distributions of (a) normalized crack opening $\bar{\delta}$, (b) gradient ξ and (c) normalized traction $\bar{p}$ along the cohesive zone, at various crack speeds for $\alpha = 1$, $\beta = 0.002$ and $m = 0.3$.

flow and damage, the stress does not exhibit a singularity, but approaches zero at the trailing edge $(x/L = 0)$ of the cohesive zone, as shown in Fig. 6c. Thus, introduction of the damage zone can solve stress divergence and discontinuity at $x/L = 0$, as mentioned by Langer and Lobkovsky (1998). The cohesive strength σ_D increases with crack growth rates. This implies an increase in stress triaxility, see Broberg (1999) and Wnuk and Legat (2002). With increasing crack speed, the crack opening and its gradient increases more rapidly in the damage zone than in the plastic zone. This is not surprising since the rate effect can suppress plastic deformation. In addition, it is shown in Fig. 6 that the solutions are insensitive to crack speed, which is below $0.5c_s$.

Fig. 7a–c show the variations of the length ratio $\overline{D}$ and aspect ratio $\bar{\delta}_c$ of the non-linear zone. With increasing crack speed, a reduction in $\overline{D}$ is detected for non-vanishing viscosity, as shown in Fig. 7a. This means that the damage zone is more deeply embedded within the plastic zone with increasing crack speed. It is expected that when the material is rate independent, $\overline{D}$ is insensitive to crack speed. Moreover, there is a reduction in the length of the cohesive zone because of an increase in the value of $\bar{\delta}_c$ as shown in Fig. 7b, since the critical crack opening displacement is specified. These trends become more evident when the crack speed is larger than $0.5c_s$.

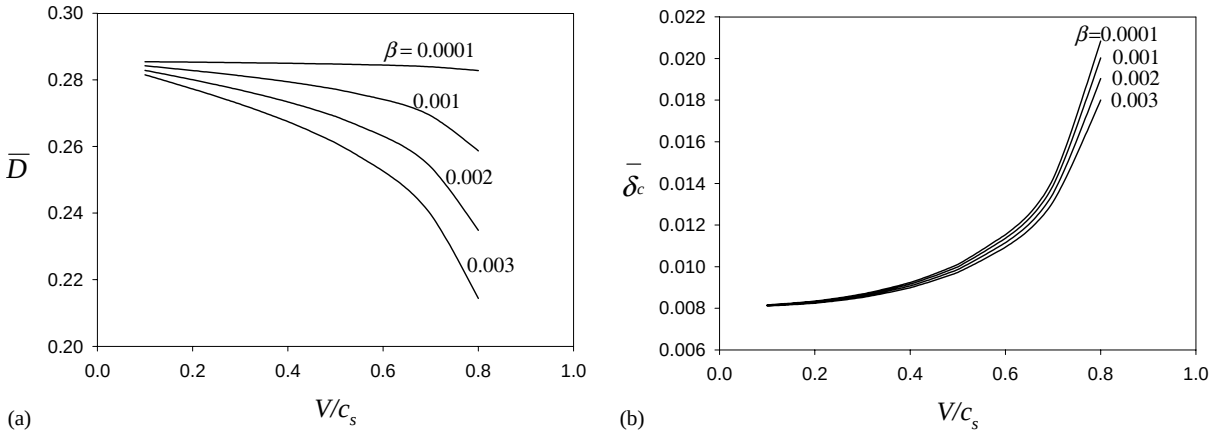

Fig. 7. Variations of (a) length ratio $\overline{D}$, and (b) aspect ratio $\bar{\delta}_c$ of the cohesive zone, at various crack speeds and β for $\alpha = 1$ and $m = 0.3$.

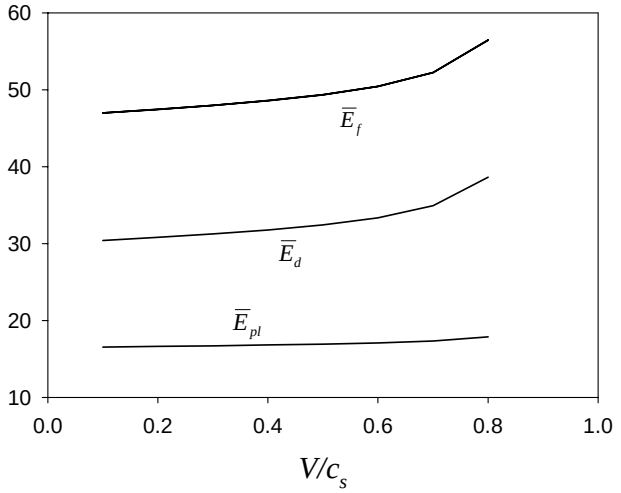

Fig. 8. Variations of normalized fracture energy $\overline{E}_f$, damage energy $\overline{E}_d$ and plastic energy $\overline{E}_{pl}$ at various crack speeds for $\alpha = 1$, $\beta = 0.002$ and $m = 0.3$.

The velocity variations of the energy components are shown in Fig. 8 for the same material parameters as in Figs. 6 and 7. The fracture energy increases with crack speed. It is seen in Fig. 8 that more energy is consumed in the damage zone than in the plastic zone. Therefore, the increase in fracture energy mainly comes from the damage zone. In contrast, the energy dissipated in the plastic zone is rather insensitive to crack speed.

5.2. Viscosity effect: β

The β-dependence of $\bar{\delta}$, ξ and $\bar{p}$ along the cohesive zone at $V/c_s = 0.5$ is shown in Fig. 9a–c. Cui (1995) demonstrated that the viscosity effect could increase the fracture stress, i.e., the cohesive strength. This conclusion is recovered here since an increase in σ_D exists as a result of an increase in viscosity. It is noted

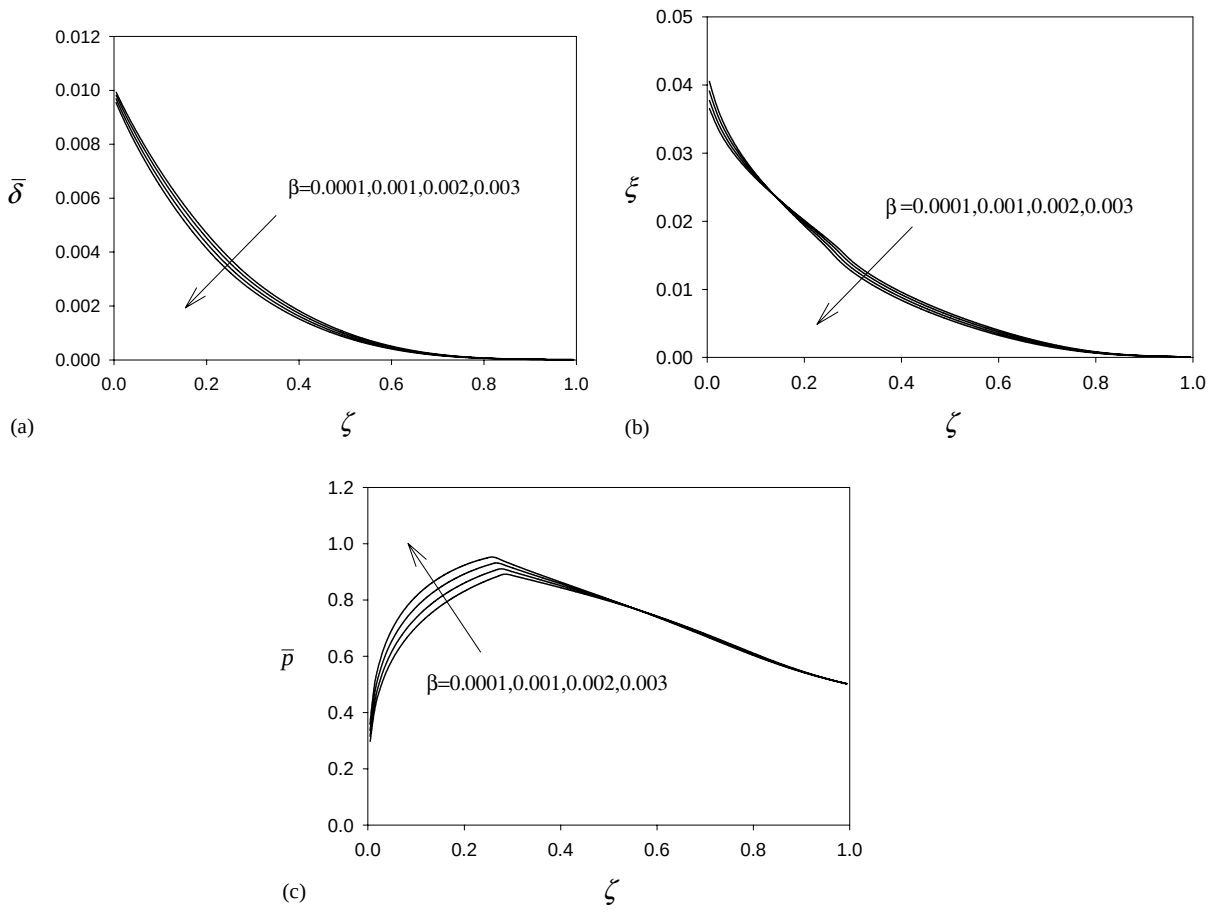

Fig. 9. Distributions of (a) normalized crack opening $\bar{\delta}$, (b) its gradient ξ and (c) normalized traction $\bar{p}$ along the cohesive zone, at various values of β for $\alpha = 1$, $V/c_s = 0.5$ and $m = 0.3$.

that the cohesive stress is enhanced in the damage zone with β. However, the viscosity effect on the opening and dislocation density is not strong.

The variations of the length ratio $\overline{D}$ and aspect ratio $\bar{\delta}_c$ of the cohesive zone are already plotted in Fig. 7 against β. Similar to the velocity effect, increasing the viscosity can reduce $\overline{D}$ so that the damage zone becomes relatively smaller compared with the plastic zone. In addition, increasing the viscosity factor can increase the length of the cohesive zone since $\bar{\delta}_c$ increases with β in Fig. 7b.

As the stress level is increased, the fracture energy can be increased by viscosity, as shown in Fig. 10a. The viscosity effect becomes more important at high crack speeds. For comparison the ratio of its plastic to damage components is shown in Fig. 10b. It is seen that the energy ratio E_{pl}/E_d decreases with increasing β. Similar to the velocity effect, increasing the viscosity coefficient makes the energy consumption in the damage zone become more dominant.

5.3. Strain-softening index: m

The shape of the cohesive law is sensitive to the choice of m and α in this model. Larger m implies faster reduction of cohesive stress in the damage zone. The variations of the length ratio and aspect ratio of the

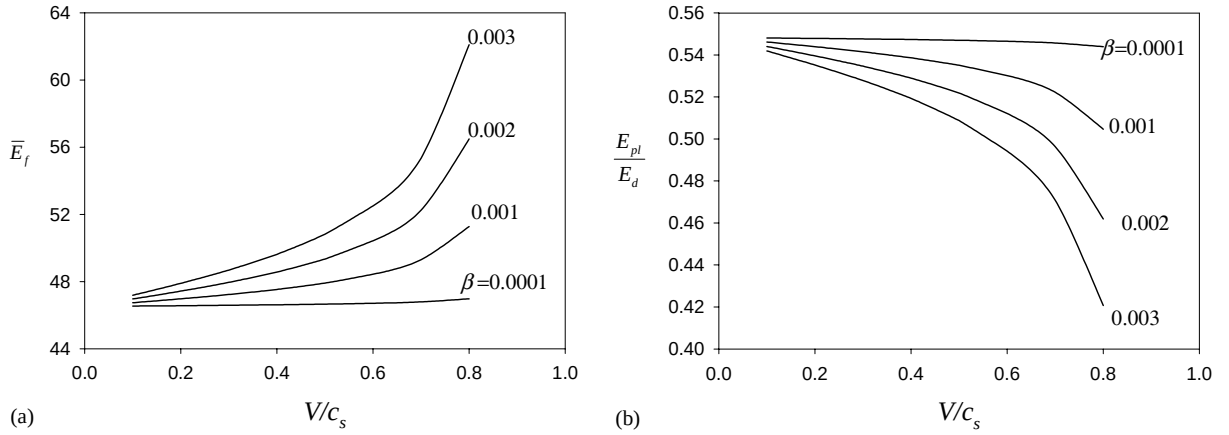

Fig. 10. Variations of (a) normalized fracture energy $\overline{E}_{\mathrm{f}}$ and (b) energy ratio $E_{\mathrm{pl}}/E_{\mathrm{d}}$ at various crack speeds and β for $\alpha = 1$ and $m = 0.3$.

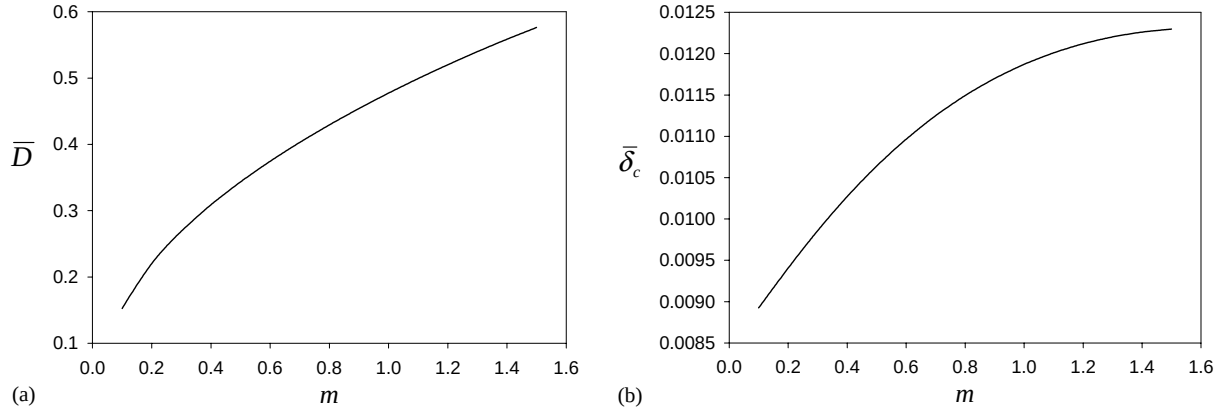

Fig. 11. Variations of (a) length ratio $\overline{D}$ and (b) aspect ratio $\bar{\delta}_{\mathrm{c}}$ of the cohesive zone at various values of m for $\alpha = 1$, $\beta = 0.002$ and $V/c_{\mathrm{s}} = 0.5$.

cohesive zone are plotted against m in Fig. 11a and b for $\alpha = 1$, $\beta = 0.002$ and $V/c_{\mathrm{s}} = 0.5$. It can be inferred from Fig. 11a that an increase in m yields a significantly larger length ratio. Considering shrinkage of the cohesive zone as $\bar{\delta}_{\mathrm{c}}$, which increases with m as shown in Fig. 11b, the plastic zone size is quite significantly reduced. As expected, the fracture energy decreases with m in Fig. 12a, and therefore, the material is vulnerable to damage. In addition, the energy contributed by the plastic zone decreases substantially with increasing m, as shown in Fig. 12b.

Fig. 13a–c show the m-dependence of $\bar{\delta}$, ξ and $\bar{p}$ along the cohesive zone for the same parameters as Figs. 11 and 12. Clearly, at a specified position ζ along the damage zone, the normalized opening increases with m, while the dislocation density or equivalently the opening rate is reduced near the physical crack-tip. From the cohesive law in the damage zone, with increasing m, this would yield a low cohesive stress at a specified position ζ, as shown in Fig. 13c. In addition, it is seen from Fig. 13c that the cohesive strength decreases with m.

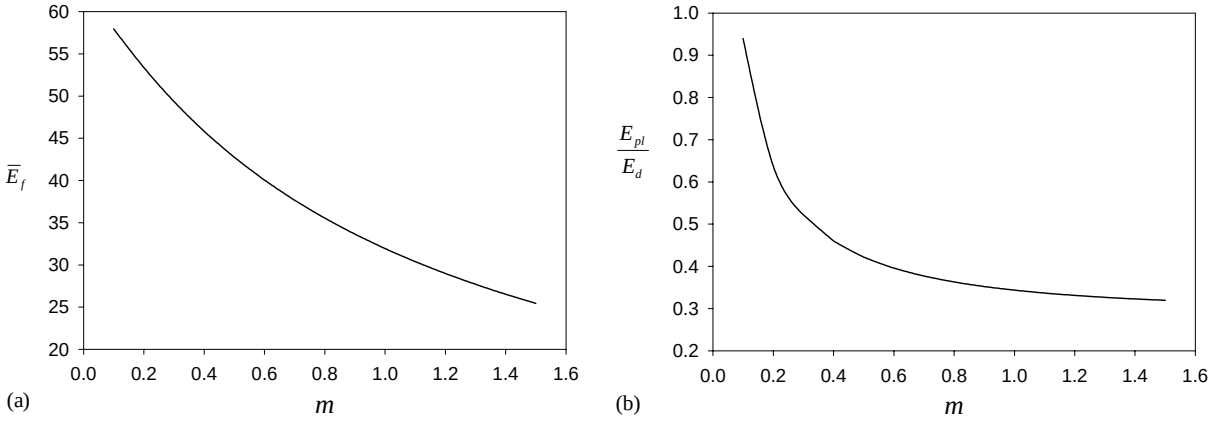

Fig. 12. Variations of (a) normalized fracture energy $\overline{E}_{\mathrm{f}}$ and (b) energy ratio $E_{\mathrm{pl}}/E_{\mathrm{d}}$ at various values of m for $\alpha = 1$, $\beta = 0.002$ and $V/c_{\mathrm{s}} = 0.5$.

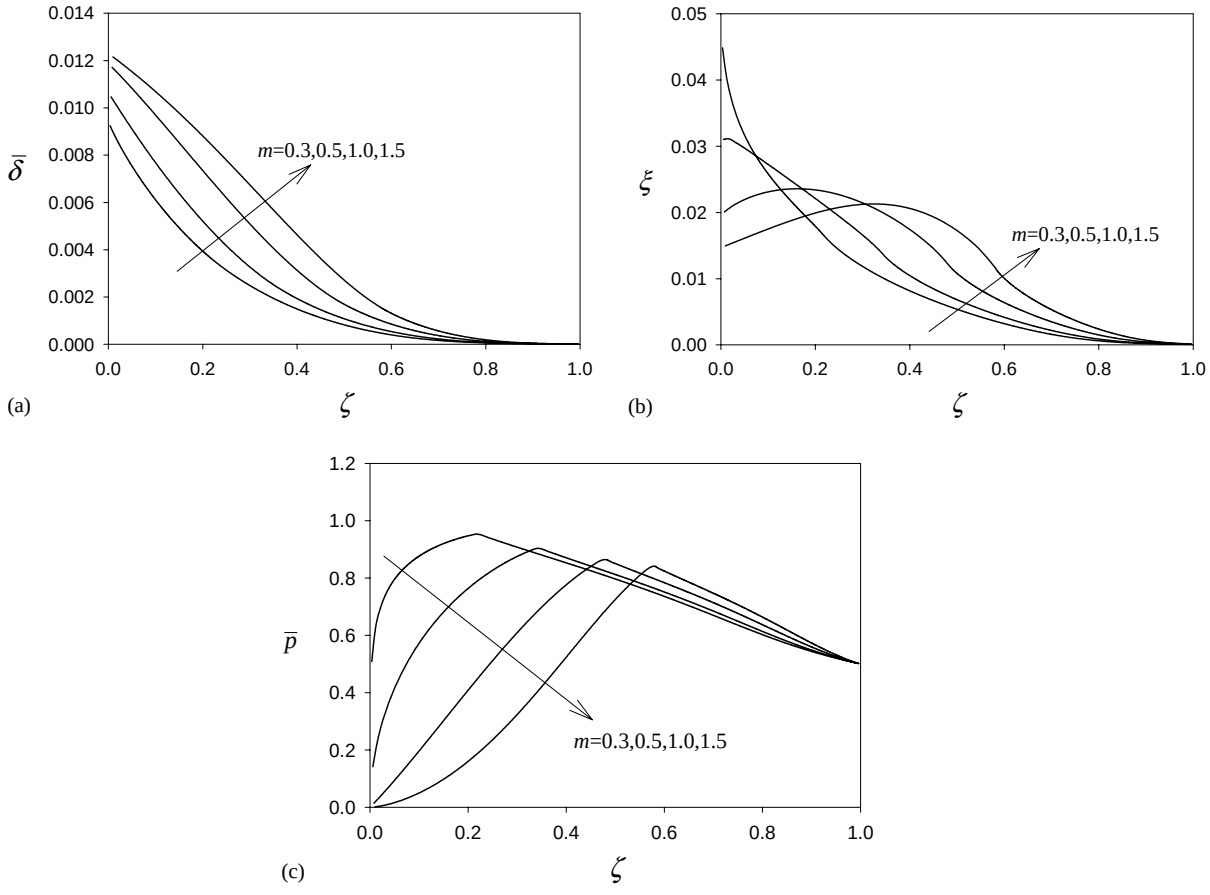

Fig. 13. Distributions of (a) normalized crack opening $\bar{\delta}$, (b) its gradient ξ and (c) normalized traction $\bar{p}$ along the cohesive zone at various values of m for $\alpha = 1$, $\beta = 0.002$ and $V/c_{\mathrm{s}} = 0.5$.

5.4. Strength ratio: $\alpha = \sigma_{pl}/\sigma_m$

Table 1 lists all global quantities at different α's for the case of $m = 0.5$, $\beta = 0.002$ and $V/c_s = 0.5$. An increase in α yields a larger $\overline{D}$ indicating the importance of the damage zone. It is found that, with

Table 1
Variations of length ratio $\overline{D}$, aspect ratio $\bar{\delta}_c$ of the cohesive zone, fracture energy $\overline{E}_f$ and energy ratio E_{pl}/E_d at various values of α for $m = 0.5$, $\beta = 0.002$ and $V/c_s = 0.5$

α	$\overline{D}$	$\bar{\delta}_c$	E_f	E_{pl}/E_d
0.8	0.231	0.0101	38.36	1.07
0.9	0.286	0.0104	40.95	0.68
1.0	0.343	0.0106	42.75	0.42
1.1	0.399	0.0108	43.94	0.24
1.2	0.449	0.0109	44.67	0.14
1.3	0.489	0.0109	45.08	0.07
1.4	0.542	0.0110	45.41	0.02

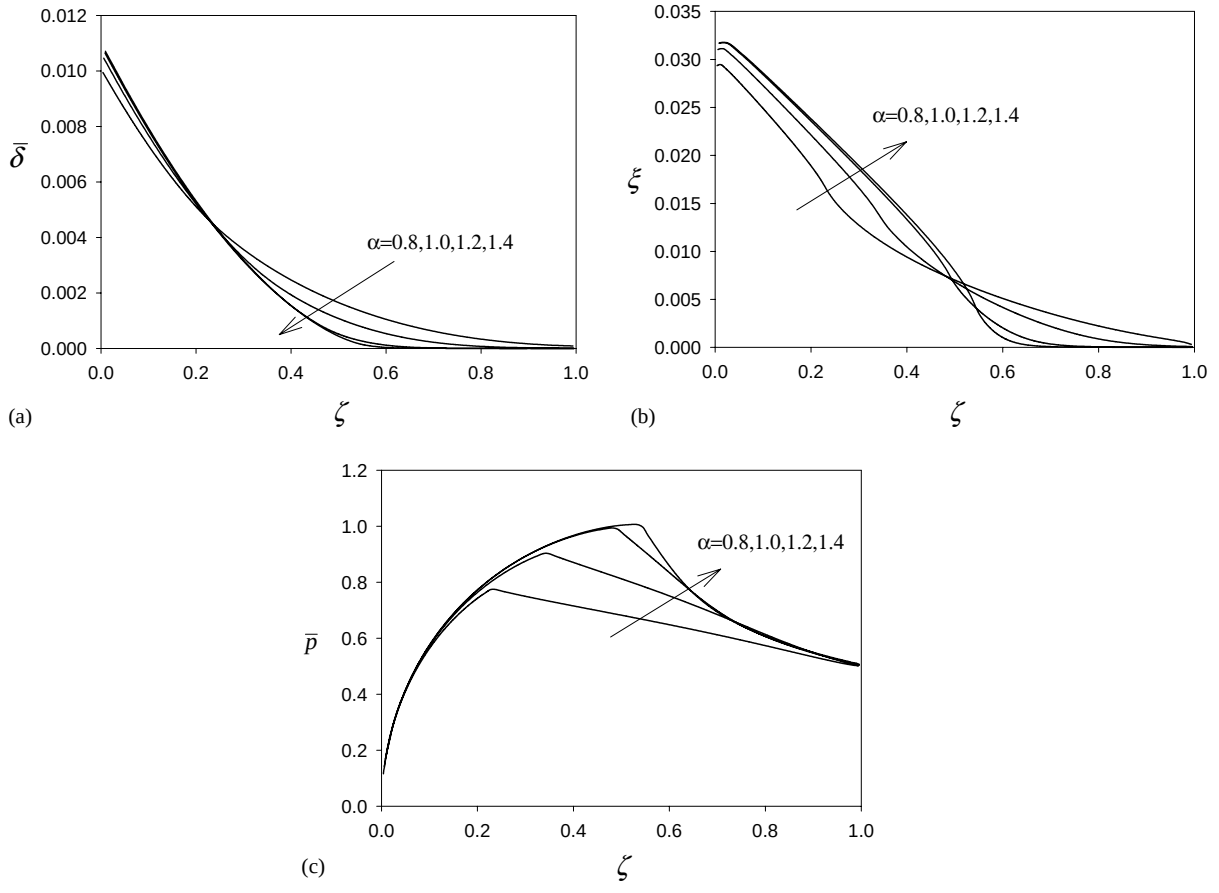

Fig. 14. Distributions of (a) normalized crack opening $\bar{\delta}$, (b) its gradient ξ and (c) normalized traction $\bar{p}$ along the cohesive zone at various α's for $m = 0.5$, $\beta = 0.002$ and $V/c_s = 0.5$.

increasing α, the fracture energy $\overline{E}_f$ increases so that the contribution to the fracture energy from the plastic zone is greatly reduced. It is noted that the length of the non-linear zone seems insensitive to the change in α, although a slight increase is found.

In this case, details about the distributions of the normalized opening, its gradient and normalized traction along the cohesive zone are provided in Fig. 14a–c. With increasing α, the opening and its gradient decrease in the plastic zone, as shown in Fig. 14a and b. At larger α's, the opening and its gradient tend to vanish in the leading parts of the plastic zone. From the traction profiles in Fig. 14c, the cohesive strength still increases with α. However, the normalized cohesive strength increases from around 0.8–1.0 while the normalized plastic ultimate strength α changes significantly from 0.8 to 1.4. Moreover, the cohesive strength tends to be steady around 1.0 with further increase in α. Thus, large fracture stress in pure plastic models, i.e., the plastic ultimate strength in this paper, cannot exist in the presence of the damage zone.

6. Conclusions

This paper presented a two-region cohesive zone model for simulating plane strain Mode-I steady-state dynamic crack growth in viscoplastic solids. Such a model, as suggested by Wnuk (1983), includes two distinct mechanisms: strain-hardening plastic flow and strain-softening damage evolution. From our results, the energy dissipated in the plastic zone clearly cannot be neglected at low crack speeds and small values of α and m. The dependence of crack growth behavior on crack speeds and cohesive constitutive parameters are addressed numerically in this paper. While the model may not capture all features of the failure of rate-dependent materials, it has provided new insights in the understanding of dynamic crack growth. Major numerical results and findings are given below.

(a) Crack growth rates can change opening and traction profiles *via* the velocity effect and rate sensitivity (viscosity). Fast crack speeds can reduce the lengths of the non-linear zone and the damage zone, but at the same time, they can increase the cohesive strength and the fracture energy. In addition, more energy is dissipated in the damage zone with increasing crack speed.
(b) Rate sensitivity (viscosity) is reflected in the effects of crack speeds, especially at high crack growth rates.
(c) The results of a small damage zone and large cohesive strength close to the physical crack-tip at high crack growth rates indicate that a critical cohesive stress can be selected as an alternative failure criterion, as stated by Costanzo and Walton (2002). With this extended criterion, it is expected that the forbidden range of crack speeds may appear for specified cohesive parameters.
(d) The definition of crack-tip constraint in rate-dependent materials needs further studies with regard to dynamic growth. Based on the cohesive strength, the increase of crack-tip constraints can be related to an increase in crack growth rates and rate-sensitivity factors. However, the increase of softening index in the damage zone can lead to the loss of constraints.
(e) Material parameters like m, n and α that control the cohesive law are affected by microstructural features like void sizes. Their physical origins are not completely understood because of a lack of microstructural studies. However, these shape parameters play an important role in fracture assessment.
(f) There is a competition between the damage zone and the plastic zone. With increasing crack speeds, the damage zone consumes more energy. Plastic energy is suppressed by crack speeds and the plastic zone length is reduced. However, the damage zone can be decreased by a lower plastic ultimate strength. In addition, even though a large ultimate strength is assigned to the plastic zone, the existence of a damage zone can lead to the lowering of the cohesive stress below the level of the plastic ultimate strength.

Acknowledgements

Parts of this work were performed when X. Zhang was a postgraduate student in the CAMT, the University of Sydney. He was in receipt of an Overseas Postgraduate Research Award tenable at the same University and an Australian Research Council (ARC) Research Scholarship. Y.-W. Mai is Federation Fellow supported by the ARC. X. Zhang and R. Jeffrey also thank the financial support from CSIRO Petroleum, Australia. Finally, the authors would like to acknowledge most sincerely the two reviewers whose constructive comments and suggestions have made this a much-improved paper.

References

Andersson, K.H., Bergkvist, H., 1970. Analysis of a non-linear crack model. J. Mech. Phys. Solids 18, 1–28.

Barenblatt, G.I., 1959. The formation of equilibrium cracks during brittle fracture: general ideas and hypothesis, axially symmetric cracks. Appl. Math. Mech. 23, 622–636.

Bilby, B.A., Cottrell, A.H., Swinden, K.H., 1963. The spread of plastic yield from a notch. Proc. R. Soc. London, A 272, 304–314.

Broberg, K.B., 1999. Influence of T-stress, cohesive strength and yield strength on the competition between decohesion and plastic flow in a crack edge vicinity. Int. J. Fract. 100, 133–142.

Costanzo, F., Walton, J.R., 2002. Steady growth of a crack with a rate and temperature sensitive cohesive zone. J. Mech. Phys. Solids 50, 1649–1679.

Cox, B.N., Marshall, D.B., 1994. Concepts for bridged cracks in fracture and fatigue. Acta Metall. Mater. 42, 341–363.

Cui, Y.L., 1995. Dynamic matrix cracking in fiber reinforced ceramics composites. J. Mech. Phys. Solids 43, 1875–1886.

Dugdale, D.S., 1960. Yielding of steel sheet containing slits. J. Mech. Phys. Solids 8, 100–104.

Fager, L.-O., Bassani, J.L., Hui, C.-Y., Xu, D.-B., 1991. Aspects of cohesive zone models and crack growth in rate-dependent materials. Int. J. Fract. 52, 119–144.

Foote, R.M.L., Mai, Y.-W., Cotterell, B., 1986. Crack growth resistance curves in strain-softening materials. J. Mech. Phys. Solids 34, 593–607.

Freund, L.B., 1990. Dynamic Fracture Mechanics. Cambridge University Press, Cambridge, UK.

Gao, H., Zhang, T.-Y., Tong, P., 1997. Local and global energy release rates for an electrically yield crack in piezoelectric ceramics. J. Mech. Phys. Solids 45, 491–510.

Glennie, E.B., 1971. A strain-rate dependent crack model. J. Mech. Phys. Solids 19, 255–272.

Hancock, J.W., Reuter, W.G., Parks, D.M., 1993. Constraint and toughness parameterised by T. In: Constraint Effects in Fracture, ASTM STP 1171. American Society for Testing and Materials, Philadelphia, pp. 21–40.

Langer, J.S., Lobkovsky, A.E., 1998. Critical examination of cohesive zone models in the theory of dynamic fracture. J. Mech. Phys. Solids 46, 1521–1556.

Muskhelishvili, N.I., 1953. Singular Integral Equations. Nordhoff, Groningen.

O'Dowd, P., Shih, C.F., 1991. Family of crack-tip fields characterized by a triaxility parameter-I. Structure of fields. J. Mech. Phys. Solids 40, 989–1015.

Press, W.H., Flannery, B.P., Teukolsky, S.A., Vetterling, W.T., 1992. Numerical Recipes. Cambridge University Press, Cambridge, UK.

Tvergaard, V., 1990. Material failure by void growth to coalescence. Adv. Appl. Mech. 27, 83–151.

Tvergaard, V., Hutchinson, J.W., 1992. The relation between crack growth resistance and fracture process parameters in elastic–plastic solids. J. Mech. Phys. Solids 40, 1377–1397.

Weertman, J., 1996. Dislocation Based Fracture Mechanics. World Scientific Publishing Co., NJ, USA.

Wnuk, M.P., 1983. Discontinuous extension of fracture in elastic-plastic deformation fields. In: Shih, C.F., Gudas, J.P. (Eds.), Elastic–Plastic Fracture Mechanics, ASTM STP 803, vol. I, pp. 159–175.

Wnuk, M.P., Kriz, R., 1985. CDM model and damage accumulation in laminated composites. Int. J. Fract. 28, 121–138.

Wnuk, M.P., Legat, J., 2002. Work of fracture and cohesive stress distribution resulting from triaxility dependent cohesive zone model. Int. J. Fract. 114, 29–46.

Yuan, H., Lin, G., Cornec, A., 1996. Verification of cohesive zone model for ductile fracture. J. Eng. Mater. Tech. 118, 192–200.

Zhangh, Ch., Gross, D., 1995. A cohesive plastic/damage zone model for ductile crack analysis. Nucl. Eng. Design 158, 319–331.